Cytoplasmic Microtubule Organizing Centers Regulate Meiotic Spindle Positioning in Mouse Oocyte

Running title: mcMTOCs regulate spindle positioning

DANIELA LONDONO VASQUEZ[1], KATHERINE RODRIGUEZ-LUKEY[1], SUSANTA K. BEHURA[1] & AHMED Z. BALBOULA[1,2]

1) Animal Sciences Research Center, University of Missouri, Columbia, MO 65211, USA

2) University of Cambridge, Department of Genetics, Downing Street, Cambridge, CB2 3EH, UK

Keywords: MTOC, Microtubule, Oocyte, Meiosis, Spindle positioning

ABSTRACT

During oocyte meiosis, migration of the spindle and its positioning must be tightly regulated to ensure elimination of the polar bodies and provide developmentally competent euploid eggs. Although the role of F-actin in regulating these critical processes has been studied extensively, little is known whether microtubules (MTs) participate in regulating these processes. Here, we characterize a pool of MTOCs in the oocyte that does not contribute to spindle assembly but instead remains free in the cytoplasm during metaphase I (metaphase cytoplasmic MTOCs; mcMTOCs). In contrast to spindle pole MTOCs, which primarily originate from the perinuclear region in prophase I, the mcMTOCs are found near the cortex of the oocyte. At nuclear envelope breakdown, they exhibit robust nucleation of MTs, which diminishes during polar body extrusion before returning robustly during metaphase II. The asymmetric positioning of the mcMTOCs provides the spindle with a MT-based anchor line to the cortex opposite the site of polar body extrusion. Depletion of mcMTOCs, by laser ablation, or manipulating their numbers, through inhibitors or inducers of autophagy, revealed that the mcMTOCs are required to regulate the timely migration and positioning of the spindle in meiosis. We discuss how forces exerted by F-actin in mediating movement of the spindle to the oocyte cortex are balanced by MT-mediated forces from the mcMTOCs to ensure spindle positioning.

38 **INTRODUCTION**

39 Mammalian oocytes enter meiosis during early fetal life. Soon after birth, meiotic oocytes
40 undergo a lengthy arrest at the dictyate stage of the prophase I of the first meiotic division (MI) [1].
41 At the age of puberty, gonadotropin cues allow prophase I-arrested oocytes to resume MI evident
42 by breakdown of the nuclear envelope (NEBD) and formation of a central bipolar spindle [2-4]. The
43 central positioning of the spindle is required to establish proper kinetochore-MT attachments and
44 to protect against aneuploidy. The position of the spindle dictates the plane of cell division [5] and
45 therefore, in contrast to mitotic cells where a centrally positioned spindle allows symmetrical cell
46 division, the meiotic spindle must migrate towards the cortex for the highly asymmetric meiotic
47 divisions [5,6]. Such peripheral positioning of the spindle is critical to extrude the tiny polar body
48 (PB) thereby retaining the great majority of the cytoplasm containing maternal RNAs and protein
49 for the egg to support early embryonic development [7,8]. It is essential to understand the critical
50 events of spindle positioning and migration, which are required for the fidelity of chromosome
51 transmission to the next generation.

52

53 To date, F-actin and its regulatory molecules represent the only cytoskeletal components known
54 to regulate spindle migration and positioning in the mammalian oocyte. It has been shown that
55 perturbation of F-actin, but not of MTs, impairs spindle migration in oocytes and that the
56 resulting increased symmetry of cell division results in infertility [6,9-11]. This contrasts with
57 mitotically dividing somatic cells, where positioning of the spindle at the center of the cell is
58 primarily regulated by the interaction of the astral MTs at its poles with the cell cortex [12]. Such
59 astral MTs are nucleated by centrosomes, centriole pairs surrounded by peri-centriolar material
60 (PCM). By contrast, mammalian oocytes lack classic centrosomes [13] because centrioles are lost

61 during early oogenesis through an unknown mechanism. The numerous acentriolar MT
62 organizing centers of the oocyte (MTOCs) [13,14] are still able to nucleate astral-like MTs but these
63 are short and unable to extend to the cortex when the spindle is centrally positioned [14-16]. These
64 observations have enforced the notion that MTs have no role in regulating central spindle
65 positioning and migration. It is therefore surprising that when mouse oocytes are treated with
66 nocodazole, a MT depolymerizing agent, chromosomes migrate towards the cortex at a higher
67 speed and at an earlier time than in control oocytes [11,17]. These unexplained observations suggest
68 that MTs have, yet unknown, role(s) in regulating spindle migration and positioning in
69 mammalian oocytes.
70
71 In prophase I-arrested oocytes, the MTOCs are initially found in the perinuclear region [13]. Then,
72 before NEBD, these perinuclear MTOCs undergo distinct processes of decondensation,
73 stretching and redistribution into a large number of smaller MTOCs [18,19]. The fragmented
74 MTOCs are then clustered and sorted to form two poles necessary to assemble a bipolar spindle
75 [14,20,21]. Another pool of MTOCs is also present in the cytoplasm during NEBD. Some of these
76 cytoplasmic MTOCs migrate from the periphery to the center of the egg, where they participate
77 in spindle formation [14,18]. Another subset of cytoplasmic MTOCs, hereafter referred to as
78 metaphase cytoplasmic MTOCs (mcMTOCs) does not contribute to spindle formation and has
79 yet unknown biological significance for oocyte meiosis.
80
81 Here, we show that the pMTOCs and the mcMTOCs of MI oocytes represent two different
82 functional sets. We find by 3D time-lapse imaging that mcMTOCs localize asymmetrically
83 opposite the site of F-actin enrichment where the polar body is extruded. Super-resolution

84 Stimulated Emission Depletion (STED) microscopy reveals that mcMTOCs are able to nucleate
85 MTs that connect the spindle to the cortex. Importantly, we show that by increasing mcMTOC
86 numbers following treatment with an inhibitor of autophagy or by depleting them by laser
87 ablation, the meiotic spindle becomes abnormally positioned leading to aneuploidy. Our results
88 suggest a model whereby the role of F-actin in mediating movement of the meiotic spindle to the
89 cortex is balanced by forces exerted from mcMTOCs to ensure the timely migration and accurate
90 positioning of the spindle in the oocyte.
91
92
93 **RESULTS**
94 **MTOCs in the cytoplasm and at the spindle poles of meiotic oocytes**
95 The multiple MTOCs of prophase I-arrested oocytes follow distinct patterns of behavior.
96 Immediately before NEBD, perinuclear MTOCs become fragmented in three phases;
97 decondensation, stretching and repositioning towards the spindle poles through the sequential
98 actions of Polo-like kinase 1, BicD2-anchored dynein, and the KIF11 motor protein [18,19]. Soon
99 after NEBD, a second group of cytoplasmic MTOCs migrates from the periphery to the center of
100 the oocyte, where it participates with perinuclear MTOCs in spindle assembly [14,18]. Finally, a
101 third population of MTOCs persists in the cytoplasm of MI oocytes at metaphase (here termed
102 mcMTOCs) [16,22-25], whose role in meiosis is unknown. To follow the behavior of mcMTOCs
103 during MI, we employed live imaging using 3D confocal microscopy to visualize prophase I-
104 arrested oocytes (collected from CF-1 mice) expressing GFP-tagged Aurora A Kinase (AURKA-
105 GFP, an integral component of MTOCs in mouse oocytes [26-28] and H2B-mCherry (H2B-mCh) to
106 label MTOCs and DNA, respectively. As previously reported, perinuclear MTOCs became

107 fragmented into small multiple MTOCs at NEBD before they sorted and re-clustered at the two
108 spindle poles as pMTOCs (Fig. 1A; Supplementary Movie 1). We also observed cytoplasmic
109 MTOCs in the cytoplasm at NEBD, some of which migrated towards the oocyte center to
110 contribute to spindle formation alongside pMTOCs whereas others, mcMTOCs remained free in
111 the cytoplasm during prophase and metaphase I (Met I) after the bipolar spindle had formed (Fig.
112 1A; Supplementary Movie 1). We carried out 3D reconstruction of entire oocytes to examine the
113 number (Fig. 1 B,C) and volume (Fig. D, E) of the mcMTOCs (Supplementary Movie 2). In
114 contrast to pMTOCs which undergo a time-dependent decrease in number and increase in
115 volume (due to MTOC clustering) as the oocyte proceeds to Met I, the mcMTOCs displayed the
116 opposite pattern and showed a time-dependent increase in number and volume in prophase and
117 Met I (Fig. 1A,B,D; Supplementary Movies 1 and 2). Each oocyte had a variable number of
118 mcMTOCs (between 4 and 12) at Met I located on different focal planes (Supplementary Movie
119 3). The mcMTOCs became less distinct, appearing to be decreased in number and volume during
120 anaphase I (Ana I) and telophase I (Telo I) before regaining their metaphase appearance as the
121 oocytes arrested in Met II (Fig. 1A-E; Supplementary Movies 1 and 2). We confirmed that these
122 AURKA-positive foci were indeed MTOCs by showing the colocalization of γ-tubulin, another
123 integral component of PCM in meiotic oocytes [20] (Supplementary Fig. 1). To confirm our
124 observations, we fixed CF-1 oocytes at different developmental stages (GV, Met I, Ana I/Telo I
125 and Met II) and immunostained them to reveal the MTOC markers, γ-tubulin, pericentrin and
126 Cep192 [18,29-31]. This also revealed pMTOCs and mcMTOCs at Met I (Fig. 1F, G) that were able
127 to nucleate asters of MTs (α-tubulin staining, Fig. 1F). Similar findings were observed in Met I
128 oocytes from C57BL/6 mice (Supplementary Fig. 2). Just as we observed in time-lapse imaging

129 of MTOCs in living oocytes, the mcMTOCs became less distinct in fixed preparations of oocytes
130 in Ana I/Telo I of fixed MI oocytes.
131
132 **mcMTOCs undergo three patterns of directional movement during MI**
133 To dissect the directional motion and kinetics of the mcMTOCs, we tracked their movement in
134 3D reconstructions over time during pro-Met I. In contrast to pMTOCs which primarily
135 originate from perinuclear MTOCs at NEBD, the mcMTOCs formed at the periphery of the
136 oocyte (Fig. 2A; Supplementary Movie 4 and 5) and then appeared to undergo three phases of
137 directional movement. In the first phase, from NEBD to early Met I, the peripheral mcMTOCs
138 moved towards the oocyte's center with an average speed of 0.09 ± 0.007 μm min^{-1} and a
139 maximum speed of 0.18 ± 0.005 μm min^{-1}. During this phase, the average volume of the
140 mcMTOCs increased, in some cases due to mcMTOCs merging with each other (Fig. 2A;
141 Supplementary Movie 4 and 5). The second was marked by the slowing of mcMTOC movement
142 to an average speed of 0.06 ± 0.009 μm min^{-1} allowing them to remain in confined areas of the
143 cytoplasm (Fig. 2B; Supplementary Movie 4). During this phase, the pMTOCs underwent active
144 clustering whereas the mcMTOCs remained apart. The third phase occurred during Ana I and
145 Telo I when the mcMTOCs showed a reversal of their behavior in phase I; they displayed a
146 drastic reduction in volume and migrated towards the cortex with an average speed of 0.12 ±
147 0.01 μm min^{-1} and a maximum speed of 0.22 μm min^{-1} (Fig. 2C; Supplementary Movies 4 and
148 6). In as many as 50% of oocytes (14/28), we were not able to observe mcMTOCs during Ana
149 I/Telo I but in all cases when they could be observed, the mcMTOCs migrated towards the
150 region of cortex opposite direction the site of extrusion of the first PB. The mcMTOCs showed
151 independent directional movement to cytoplasmic droplets and so do not reflect overall

152 cytoplasmic movements (Supplementary Fig. 3). Taken together, our observations confirm that
153 meiotic oocytes have two different pools of MTOCs and suggest that mcMTOCs differ from
154 pMTOCs in their function.
155
156 **mcMTOCs localize asymmetrically to anchor the spindle to the cortex**
157 To determine whether the mcMTOCs were physically connected to pMTOCs, we employed
158 immunocytochemistry and STED super-resolution microscopy to visualize the MTOCs in
159 relation to MTs and F-actin. We confirmed that F-actin formed a cage around the spindle as
160 previously reported [10,32] but could not detect any direct connection of F-actin between the
161 pMTOCs and mcMTOCs (Supplementary Fig. 4). In contrast, we detected MTs originating from
162 the mcMTOCs and linking them to both the oocyte cortex and the pMTOCs and spindle (Fig.
163 3A,B). In addition, we also observed MTs connecting mcMTOCs with each other. Relatively
164 short astral-like MTs could not reach the oocyte cortex unless they bind mcyMTOCs
165 (Fig. 3A,B). Thus, mcMTOCs enable MTs to bridge the gap between the spindle and the
166 cortex. It was also evident from our observations that the mcMTOCs were asymmetrically
167 distributed in the oocyte cytoplasm leading us to consider their relationship in time and space to
168 the positioning of the spindle itself. In prophase arrest oocytes, the GV is usually found in a
169 centralized location [33-36]. Consequently, the spindle also forms around the chromatin at or near
170 the center of the oocyte before it migrates towards the cortex in late pro-Met to allow
171 asymmetrical cell division. In all the oocytes examined, we found that the mcMTOCs were all
172 asymmetrically positioned from the GV stage and throughout NEBD and early pro-Met I when
173 the spindle is still localized centrally (Fig. 3C; Supplementary Movie 7). Strikingly, when the
174 spindle began its actin-mediated migration, this took place towards the opposite side of the

175 oocyte to that occupied by mcMTOCs in the majority of the oocytes (38 out of 40 examined, Fig.
176 3 C-E). These findings suggest a model whereby mcMTOCs localize asymmetrically to anchor
177 the spindle to the cortex in such a way as to oppose the F-actin mediated force that builds to
178 direct the spindle to the cortex on the opposite face of the oocyte for polar body extrusion. This
179 would account for the unexplained finding that nocodazole-induced MT depolymerization during
180 Met I results in the earlier migration of chromosomes towards the cortex at a relatively higher
181 speed than in control oocytes (Supplementary Fig. 5) and others [11]. Thus, the mcMTOCs appear
182 to enable opposing MT forces that counter spindle/chromosome migration that are necessary to
183 regulate its timing and the final position of the spindle.
184
185 **mcMTOCs regulate spindle positioning in acentriolar oocytes**
186 To determine the function(s) of mcMTOCs during MI and to test the above hypothesis, we
187 selectively depleted mcMTOCs by two-photon laser ablation (Fig. 4A). The two-photon laser
188 microscope has the advantage of offering deeper tissue penetration enabling efficient ablation
189 and minimizing off-target effects [37]. We first microinjected prophase I-arrested oocytes with
190 cRNAs encoding *Aurora A-GFP* and *eGFP-EB3* to label MTOCs and MTs, respectively. We
191 then marked small cuboidal regions surrounding each mcMTOC, which we then exposed to a
192 927 nm wavelength laser to ablate the mcMTOCs, (Fig. 4B; Supplementary Movie 8). We
193 ensure reduction of fluorescence of each mcMTOC to background levels (compare images
194 before ablation, Fig. 4B, upper panels, to after ablation, Fig. 4B, lower panels) before ablating
195 the next. Importantly, laser ablation not only depleted the mcMTOCs but also disrupted their
196 associated nucleation of MTs (Fig. 4C). We also exposed control oocytes to the same protocol by
197 ablating random areas of the cytoplasm adjacent to but not overlapping with the mcMTOCs.

198 We confirmed the efficiency of mcMTOC depletion by immunostaining a subset of oocytes to
199 reveal γ-tubulin and were only able to detect γ-tubulin foci in the cytoplasm but not at spindle
200 poles (Supplementary Fig. 6). Control and mcMTOC-depleted oocytes were *in vitro* matured for
201 16 h allowing us to assess the proportion of Met II eggs and determine their karyotype using an
202 *in situ* chromosome counting technique [38,39]. We first noted that the depletion of mcMTOCs
203 resulted in a significant increase in oocytes arrested at Met I compared to control oocytes (Fig.
204 4D). Importantly, a relatively higher proportion of mcMTOC-depleted eggs were aneuploid (7
205 out of 13 examined eggs) compared to controls (6 out of 24 examined eggs). Because depletion
206 of mcMTOCs increased the percentage of oocytes arrested at Met I stage (Fig. 4D), we were not
207 able to assess spindle positioning due to the high variability related to the meiotic stage and so
208 we chose to arrest meiotic progression in Met I by incubating oocytes in meiotic maturation
209 medium containing a proteasome inhibitor (MG-132). In this way, we could compare spindle
210 positioning in such arrested oocytes (Fig. 4A). This revealed that whereas in control MI arrested
211 oocytes, the spindle maintained its position over a period of 8h, the position of the spindle in
212 mcMTOC-depleted oocytes was not stable (Fig. 4e; Supplementary Movie 9 and 10) and
213 displayed considerable movement (Fig. 4F,G). Following the onset of spindle movement in
214 mcMTOC-depleted oocytes, the spindle poles lost their integrity in contrast to control oocytes,
215 likely due to the imbalance of forces on spindle poles (Supplementary Movie 9 and 10). Together
216 this suggests that the mcMTOCs are required to position the MI spindle and maintain the
217 integrity of the spindle poles.
218
219
220

221 **Autophagy regulates mcMTOC numbers and spindle positioning in meiotic oocytes**

222 In mitotic cells, autophagy plays an important role in regulating and maintaining the proper
223 number of centrosomes where autophagy-deficient cells contained multiple centrosomes [40,41].
224 This led us to investigate the effects of inhibiting or inducing autophagy upon mcMTOC
225 numbers and the consequences for meiosis. To this end, we chose to treat oocytes with 3-
226 Methyladenine (3-MA), which inhibits autophagy by blocking autophagosome formation via the
227 inhibition of type III Phosphatidylinositol 3-kinases (PI-3K). However, because 3-MA
228 (autophagy inhibitor) blocks NEBD (data not shown), we treated oocytes with 3-MA
229 immediately after NEBD. We also treated oocytes with rapamycin as an inducer of autophagy
230 by adding the compound to the *in vitro* maturation medium during prophase I. In both cases, we
231 allowed the treated oocytes (3-MA or rapamycin) together with controls to mature for 5 h post-
232 NEBD prior to fixation and immunostaining using anti-Cep192 and anti-α-tubulin antibodies to
233 label MTOCs and the spindle, respectively. We found that treatment with rapamycin resulted in a
234 decrease in the number of mcMTOCs, compared to control oocytes (Fig. 5A-C). In contrast,
235 treatment with 3-MA significantly increased the number of mcMTOCs, but not pMTOCs,
236 compared to control oocytes (Fig. 5d-f). To determine the effect of such drug treatments upon
237 spindle positioning, we used DIC imaging to track the position of chromosomes over time.
238 Rapamycin-treated oocytes behaved in a similar way to controls; we could see no significant
239 differences in the proportion of oocytes completing MI and extruding a polar body (Fig. 6A,B).
240 Moreover, rapamycin-treated oocytes showed no differences to controls in chromosome
241 positioning (Fig. 6A,F; Supplementary Movie 11 and 12), in the average time spent by
242 chromosomes during migration to reach the cortex (Fig. 6C), in the total distance traveled by
243 chromosomes until reaching the cortex; Fig. 6D), or in the average speed of migrating

244 chromosomes (Fig, 6E). By contrast, the increase in MTOC numbers following 3-MA treatment
245 was associated with abnormal chromosome (spindle) positioning and orientation (Fig. 6A,F;
246 Supplementary Movie 13 and14) with chromosomes moving in circles in around 40% of oocytes
247 treated with 3-MA. Accordingly, we found a significant increase in the distance traveled by
248 chromosomes during migration until reaching the oocyte cortex (Fig. 6D). In line with our model
249 that mcMTOC-mediated MTs anchor the spindle to the cortex opposite the PBE side to position
250 the spindle centrally, we found that increasing mcMTOC numbers by 3-MA treatment resulted in
251 a significant delay in chromosome migration towards the cortex (Fig. 6C), resulting from their
252 significantly ($p < 0.001$) reduced speed (Fig. 6E) in comparison to control oocytes. Indeed, we
253 observed cases in which the chromosomes underwent segregation before the spindle had reached
254 the cortex, resulting in enlarge polar bodies in around 21.05% of oocytes (Supplementary Movie
255 14). The relatively weaker effect of rapamycin than 3-MA on spindle positioning could be
256 attributed to our observation that average mcMTOC number in rapamycin-treated oocytes (~ 4)
257 remained within the range of mcMTOC numbers in control oocytes (between 4 and 12).
258 Together, these data show that mcMTOC numbers must be regulated tightly, and provide further
259 evidence that mcMTOCs play an important role in regulating the spindle position and timing of
260 its migration in mouse oocytes.
261

262 **DISCUSSION**

263 To date, the only known function of acentriolar MTOCs in mouse oocytes is to assemble the
264 spindle. Using 3D time-lapse confocal microscopy, we identify a subset of MTOCs that remain
265 free in the cytoplasm during Met I of meiosis and which do not contribute to bipolar spindle
266 assembly *per se*. In contrast to polar pMTOCs, which originate mainly from the perinuclear

267 MTOCs in prophase I, the mcMTOCs originate exclusively from MTOCs present in the
268 cytoplasm in prophase I. The mcMTOCs are first observed near the oocyte cortex at NEBD; they
269 increase in number and size while moving to a central position during Met I. STED super-
270 resolution microscopy revealed that microtubules nucleated by the mcMTOCs connect one side
271 of the spindle to the cortex during Met I. In Ana I/Telo I of MI, the mcMTOCs undergo a
272 decrease in both number and size while migrating towards the cortex. When mcMTOCs
273 functions were perturbed, either by laser ablation or treatment with 3-Methyladenine (3-MA) to
274 inhibit type III Phosphatidylinositol 3-kinases and increase MTOC numbers, we have shown that
275 the mcMTOCs play a role in regulating spindle positioning and the timing of its migration to the
276 cortex.
277
278 To our knowledge, this is the first study of the function of mcMTOCs in living mammalian
279 oocytes, which differ in several ways from the pMTOCs. The majority of pMTOCs, for
280 example, originate from the perinuclear MTOCs, which never contribute to the mcMTOCs.
281 Whereas the pMTOCs undergo a clustering-associated decrease in number and increase volume
282 During pro-Met I/Met I, the mcMTOCs undergo a steady increase in both number and volume
283 and rarely self-aggregate (~1.5% of all examined mcMTOCs). Interestingly, inhibition of
284 autophagy with 3-MA increased the number of mcMTOCs, but not pMTOCs. Finally, in contrast
285 to pMTOCs, mcMTOCs participated in spindle positioning but never contributed to bipolar
286 spindle assembly. Together, these observations suggest that mammalian oocytes have two
287 different functional sets of MTOCs and raise the future important challenge to determine
288 whether differences in their biochemical compositions underlie their differences in function.
289

290 The primary function of the spindle is to provide the machinery for faithful chromosome
291 segregation. This is achieved in a series of critical, non-overlapping steps. First, during pro-Met I
292 and early Met I, the spindle is assembled and positioned at or near the oocyte's center. Second,
293 during the late Met I, the spindle migrates towards a sub-cortical location to allow asymmetrical
294 cell division. Third, the spindle rotates from a parallel to a perpendicular position in relation to
295 the cortex to allow PB extrusion. Many studies have emphasized the roles of F-actin and its
296 motor proteins in regulating spindle positioning and migration [9-11] and two models have been
297 proposed to explain how F-actin regulates spindle positioning and migration. In the first, F-actin
298 enrichment at the cortex provides a spindle pulling force [9]. In the second, a spindle pushing force
299 is mediated by the cytoplasmic F-actin meshwork [11]. Both models enforce the notion that an F-
300 actin-mediated force on the spindle, whether pushing or bulling, acts towards the nearest cortical
301 side through which the PB is extruded. On the other hand, spindle orientation seems to be
302 dependent on both F-actin and MTs [15]. Astral-like MTs are only able to reach the cortex only
303 when it is very close to the spindle poles [15]. Because astral-like MTs are relatively short and
304 cannot easily reach the cortex, they can only establish contacts with MTs nucleated by
305 mcMTOCs which, in turn, could act as amplifying sites that anchor the spindle to the cortex.
306 This model, which we here propose, thus depends on the presence of two opposing forces:
307 cyMTOC-mediated MTs at one side and F-actin at the other side of the spindle (Fig. 6). These
308 opposing forces would be essential to position the spindle centrally during early Met I and to
309 prevent premature spindle migration. Our model is consistent with three sets of observations: 1)
310 mcMTOCs are exclusively localized asymmetrically, opposite the site of PB extrusion (the side
311 of F-actin enrichment); 2) mcMTOCs undergo a significant decrease in number and volume
312 during late Met I and Ana I/Telo I, allowing the F-actin mediated force to extrude the PB; and 3)

313 nocodazole-mediated MT depolymerization advances the timing of chromosome migration to the
314 cortex, which takes place at a relatively higher speed [11,17] whereas increasing mcMTOC numbers
315 delays chromosome migration to the cortex, which occurs at a relatively reduced speed compared
316 to controls.
317
318 Depletion of mcMTOCs, disruption of mcMTOC numbers and MT depolymerization were each
319 associated with abnormal spindle positioning and/or perturbed chromosome/spindle migration.
320 For example, increasing mcMTOC numbers by 3-MA treatment significantly decreased
321 chromosome speed and delayed chromosome migration towards the cortex. This phenotype
322 accords with increased mcMTOC-mediated MT forces that oppose F-actin; thereby preventing
323 proper spindle migration. Conversely, depleting mcMTOCs using laser ablation or MT
324 depolymerization has the reciprocal effect [11,17]. These findings indicate that the numbers of
325 mcMTOCs must be regulated tightly to regulate spindle positioning and timely spindle
326 migration.
327
328 In almost all mammals, including humans [42,43], meiotic oocytes contain numerous acentriolar
329 MTOCs. This is in contrast to somatic mitotic cells, which contain only a pair of centrosomes
330 that are sufficient to assemble and position the spindle centrally. Positioning the spindle at the
331 center of mitotic cells depends on nucleating symmetrical astral MTs that anchor the spindle to
332 the cell cortex. However, the mechanism appears different during MI. Mammalian eggs are large
333 and the astral MTs from acentriolar MTOCs are relatively short. Yet, the cell must divide
334 asymmetrically, something that would likely be difficult for a pair of symmetrical centrosomes to

335 achieve. Our proposed model may, therefore, account for why meiotic oocytes rely upon two
336 different functional sets of numerous MTOCs rather than a pair of typical centrosomes.
337
338 **MATERIAL AND METHODS**
339 **Ethics**
340 All animals were kept and experiments were conducted in accordance with UK Home Office
341 regulations and the University of Missouri (Animal Care Quality Assurance Ref. Number, 9695).
342
343 **Oocyte collection, microinjection and culture**
344 Full-grown GV-arrested oocytes were isolated from CF-1 or C57BL/6 female mice (6-8-week-
345 old) previously primed (~44 h before collection), with pregnant mare serum gonadotropin (Lee
346 BioSolutions #493-10-10) according to [44,45]. Unless otherwise specified, CF-1 mice were used to
347 conduct the experiments. Cumulus oocyte complexes (COCs) were collected and denuded using
348 mechanical pipetting in bicarbonate-free minimal essential medium (MEM) containing 3 mg/ml
349 polyvinylpyrolidone (PVP) and 25 mM Hepes (pH 7.3) supplemented with 2.5 μM milrinone
350 (MilliporeSigma, St. Louis, MO, USA # M4659), a phospho diesterase inhibitor to arrest the
351 oocytes at prophase I [46]. Prophase I-arrested oocytes were microinjected with 10-15 pl of cRNAs
352 encoding fluorescently labeled proteins while cultured in milrinone-containing MEM medium.
353 Microinjected oocytes were then cultured in Chatot, Ziomek, and Bavister (CZB) medium [47]
354 supplemented with milrinone in a humidified incubator with 5% CO_2 in air at 37°C for ~3 h to
355 allow protein expression before releasing into milrinone-free CZB medium and initiating *in vitro*
356 maturation. Met I, Ana I/Telo I or Met II oocytes were collected at 4, 7 or 14 h after NEBD.

357 Nocodazole (MilliporeSigma #M1404), MG-132 (MilliporeSigma #474790), Rapamycin (Enzo
358 Life Sciences, Farmingdale, NY, USA #BML-A275), 3-Methyladenine (3-MA, Cayman
359 Chemical, Ann Arbor, MI, USA #13242) were dissolved in dimethyl sulfoxide (DMSO) and
360 used at a final concentration of 7.5 μM, 20 μM and 10 mM, respectively. *In vitro* maturation was
361 carried out in organ culture dishes under humidified conditions (Becton Dickinson #353037).
362

363 **Cloning and *in vitro* cRNA synthesis**

364 Generation of *Aurka-Gfp*, *H2b-mCherry* and *eGfp-Eb3* were described previously [28,48]. DNA
365 linearization of *Aurka-Gfp* and *H2b-mCherry* constructs was carried out using Nde I (New
366 England BioLabs), whereas DNA linearization of *eGfp-Eb3* construct was carried out using SfiI
367 (New England BioLabs). Purification of linearized DNA was carried out according to the
368 manufacturer's protocol (Qiagen, QIAquick PCR Purification). Purified DNA was *in vitro*
369 transcribed using an mMessage mMachine T7 kit (Ambion) to generate *Aurka-Gfp* and *H2b-*
370 *mCherry* cRNAs or mMessage mMachine T3 kit (Ambion) to generate eGfp-Eb3 cRNA
371 according to the manufacturer's instructions. cRNA purification was performed using an
372 RNAEasy kit (Qiagen) and stored at −80°C.
373

374 **Immunocytochemistry and fluorescence microscopy**

375 Meiotic oocytes were fixed for 20 min at room temperature in freshly prepared 2 %
376 paraformaldehyde solution (MilliporeSigma #P6148) dissolved in phosphate buffer saline (PBS).
377 Fixed oocytes were permeabilized in 0.1% Triton X-100 in PBS for 20 min prior to incubation
378 for an additional 20 min in PBS containing 0.3% BSA and 0.01% Tween-20 (blocking solution).
379 Primary antibody incubation was performed at room temperature for 1 h. Oocytes were then

380 washed three times (8-9 min each) prior to incubation with secondary antibodies for 1 h. Oocytes
381 were washed again three times in blocking solutions for 8-9 min. To detect F-actin, phalloidin
382 (Texas Red X Phalloidin, ThermoFisher Scientific #T7471; 1:50) was added to secondary
383 antibody solutions. Oocytes were mounted on slides using Vectashieled with 4',6-Diamidino-2-
384 Phenylindole, Dihydrochloride (DAPI; Vector Laboratories, Burlingame, CA, USA) to stain
385 DNA. To label DNA for STED super-resolution imaging, 5 mg/m Hoechst 33342 was used
386 (Molecular Probes H3570). The following primary antibodies were used in immunofluorescence:
387 α-tubulin-Alexa Fluor 488 conjugate (Life Technologies #322 588; 1:100), Cep192 (Young In
388 Frontier #AR07-PA0001; 1:100), γ-tubulin (Millipore-Sigma #T6557; 1:75), Pericentrin (BD
389 Biosciences #611814; 1:100), CREST autoimmune serum (Antibodies Incorporated #15-234;
390 1:25). Omitting the primary antibody served as a negative control. Fluorescence signals were
391 detected under a 63X objective using Leica TCS SP8 confocal microscope equipped with 3-
392 color, 3-D STED super-resolution 3X system. Images were captured to span the entire oocyte at
393 3 µm Z-intervals (confocal microscopy) or 0.5 µm Z-intervals (STED super-resolution
394 microscopy). All images were acquired using the same laser power when the intensity of
395 fluorescence is quantified.
396
397 **Time-lapse confocal microscopy**
398 Oocytes expressing fluorescently labeled proteins were transferred to milrinone-free CZB
399 medium and imaged over time under a 63X objective using Leica TCS SP8 confocal microscope
400 equipped with microenvironmental chamber to maintain the oocytes at controlled CO_2 (5%) and
401 temperature (37 °C) in a humidified air. DIC, GFP and mCherry image acquisitions were started
402 at prophase I stage and images were captured every certain time according to each experimental

403 design (as indicated in corresponding figure legends). Images were captured to span the entire
404 region including all MTOCs at 3 μm Z-intervals.
405
406 **Depletion of mcMTOCs using laser ablation**
407 Depletion of mcMTOCs was carried out using two-photon laser ablation which has the
408 advantage of offering deeper tissue penetration, efficient ablation and minimizing off-target
409 effects [37]. Two different microscopes were used. Oocytes expressing fluorescently labeled
410 proteins were transferred to milrinone-free MEM medium and mcMTOCs were ablated using
411 upright LaVision BioTec TriM Scope II (with controlled temperature at 37 °C) or to milrinone-
412 free CZB medium if Leica TCP SP8 two-photon inverted microscope (equipped with
413 microenvironmantal chamber to control CO_2 and temperature) was used. In both cases, a small
414 square area(s) surrounding mcMTOCs were marked and then exposed to a laser with 927 nm
415 wavelength. We compared the first image (before ablation) and the second image (after ablation)
416 in the time series cycle to ensure that after ablation, the fluorescence in the targeted mcMTOCs
417 decreased to that observed at the background levels. Next, we moved the focal plane and ablated
418 the remaining mcMTOCs. McMTOC-depleted oocytes underwent live imaging using the same
419 parameters. Control oocytes were exposed to the same protocol except ablating random areas of
420 the cytoplasm, just adjacent and equal to the same size and number of mcMTOCs.
421
422 **Image processing and analysis**
423 Images acquired using 3-D STED super-resolution microscopy were deconvolved using Huygens
424 Professional software before image analysis. NIH image J software (National Institute of Health,
425 Bethesda, MD, USA) was used to process and analyze the images of fixed oocytes. The speed

426 and average distance of chromosome/spindle/MTOCs at their final position over time were
427 analyzed using the manual tracking function of NIH image J software. The point of intersection
428 between the line connecting the two dominant spindle poles and spindle midzone was used to
429 determine the position of the spindle. The point of intersection between the two lines
430 representing the minor axis length and the major axis length of chromosomes was used to
431 determine the position of all chromosomes [49]. The speed and distance for each MTOC were
432 analyzed separately before calculating the average for all MTOCs within each oocyte. 3D
433 reconstruction of MTOCs, MTOC number and volume were processed and analyzed using
434 isosurface spot analysis feature of Imaris software (Bitplane, Zürich, Switzerland) according to
435 [18]. Briefly, based on MTOC signal to noise, the threshold value was adjusted on an oocyte-to-
436 oocyte basis followed by MTOC surface segmentation. MTOC number was calculated using the
437 spot analysis feature, whereas MTOC volume was analyzed using surface analysis feature.
438 mcMTOCs were quantified after excluding the pMTOCs manually, and *vice versa*. Same
439 processing parameters were applied for each experimental analysis
440

441 ***In situ* chromosome counting**

442 Oocytes at Met II stage (12 h post-NEBD) were treated with 100 μM monastrol (MilliporeSigma
443 #M8515), an Eg5-kinesin inhibitor to induce monopolar spindle formation with subsequent
444 chromosome dispersion [38,39]. Oocytes were fixed and immunostained by Cep192, pericentrin, as
445 previously mentioned with CREST autoimmune serum to detect kinetochores. Oocytes were then
446 mounted onto a glass slide using Vectashield with DAPI (Vector Laboratories) to label DNA.
447 Confocal microscopy was used to image the entire region of the chromosomes at 0.7-μm Z-

intervals to capture all kinetochores. Serial confocal sections were analyzed and the total number of kinetochores were counted using NIH image J software.

Statistical analysis

One-way ANOVA, Student t-test and chi-square contingency test were used to evaluate the differences between groups using GraphPad Prism. ANOVA test was followed by the Tukey post hoc test to allow the comparison among groups. The differences of $P < 0.05$ were considered significant. The data were expressed as means ± SEM.

FUNDING

This study was supported by Marie Sklodowska-Curie Fellowship 706170, Horizon 2020, European Commission and laboratory start-up funding from the University of Missouri to AZB.

ACKNOWLEDGMENTS

The authors would like to thank Dr. David Glover, California Institute of Technology, USA for critical reading and editing the manuscript, and for providing resources. The authors would like to thank all members of the Glover lab and the Balboula lab for valuable help and discussions.

DECLARATION OF INTEREST

The authors declare that there is no conflict of interest that could be perceived as prejudicing the impartiality of the research reported.

472 **FIGURE LEGENDS**

473 **Figure 1: Two different sets of MTOCs are present in acentriolar oocytes.** (A) Time-lapse
474 confocal microscopy of MTOCs in live oocytes. Full-grown prophase-I oocytes were injected
475 with cRNAs encoding *H2b-mCherry* (red) and *Aurka-Gfp* (pseudo white), incubated in
476 milrinone-containing CZB medium for 3 h, followed by *in vitro* maturation. Shown are
477 representative images (Z-projection of 16 sections every 3 μm) from a time course (see
478 Supplemental Movie 1). Lower panels represent a 3D reconstruction of MTOCs from oocyte
479 shown in upper panels (see Supplemental Movie 2). Fluorescence images were captured every
480 20 min (time, h:min). The scale bar represents 10 μm. The white arrow represents cytoplasmic
481 MTOC that participate in spindle pole formation as a pMTOC. White arrowhead represents
482 cytoplasmic MTOC that remains in the cytoplasm during Met I (mcMTOC). (B,D)
483 Quantification of average MTOC number and MTOC volume over time during meiosis I,
484 respectively. Error bars show S.D. Dashed blue lines represent the time of Ana I onset. (C,E).
485 Quantification of average MTOC number and MTOC volume, respectively, during metaphase I
486 (Met I) and anaphase I/telophase I (Ana I/Telo I) stages. The data are expressed as mean ± SEM.
487 Student t-test was used to analyze the data. Values with asterisks vary significantly, ****P <
488 0.0001. The total number of analyzed oocytes (from three independent replicates) is specified
489 above each graph. (F) Fully grown prophase-I-arrested oocytes were *in vitro* matured for 0 (Pro
490 I, prophase I), 8 h (Met I), 9 h (Ana I/Telo I) or 16 h (Met II) prior to fixation and
491 immunocytochemistry using γ-tubulin and α-tubulin antibodies to label MTOCs (red) and
492 microtubules (grey). DAPI was used to detect DNA (blue). (G) Fully grown prophase-I-arrested
493 oocytes were *in vitro* matured for 8 h (Met I) followed by fixation and immunostaining using
494 Cep192 (red) and pericentrin (grey) antibodies to label MTOCs. DAPI was used to detect DNA

495 (blue). Shown are representative confocal z-projections. Arrowheads represent mcMTOCs. A
496 total of 184 oocytes were examined. Scale bars represent 10 µm.
497
498 **Figure 2: mcMTOCs exhibit three different directional behaviors during meiosis I.**
499 Tracking of 3D reconstructed mcMTOCs from time-lapse confocal microscopy in live oocytes
500 during three different phases: (A) nuclear envelope breakdown (NEBD)- early metaphase I (Met
501 I, see Supplemental Movie 4 and 5), (B) Met I (see Supplemental Movie 4) and (C) late Met I-
502 telophase I (Telo I), see Supplemental Movie 5 and 6. Full-grown prophase-I oocytes were
503 injected with cRNAs encoding *H2b-mCherry* (red) and *Aurka-Gfp* (pseudo white), incubated in
504 milrinone-containing CZB medium for 3 h prior to *in vitro* maturation. Shown are representative
505 images of 3D reconstructed Z-projection of 16 sections every 3 µm from a time course.
506 Fluorescence images were captured every 15 min (time, h:min). The scale bar represents 20 µm.
507 Right panels show a zoomed area of mcMTOC tracking over time. White arrows represent the
508 overall direction of displacement calculated automatically by Bitplane Imaris software.
509 Arrowheads represent mcMTOCs. The total number of analyzed oocytes is 34.
510
511 **Figure 3: mcMTOCs anchor the spindle to the cortex.** (A) Fully grown prophase-I-
512 arrested oocytes were *in vitro* matured for 6 h (metaphase I) prior to fixation and
513 immunocytochemistry using γ-tubulin and α-tubulin antibodies to label MTOCs (red) and
514 microtubules (grey). Hoechst was used to detect DNA (blue). Fluorescence signals were detected
515 under a 63X objective using STED super-resolution system. Shown is a representative image (Z-
516 projection of 65 sections every 0.5 µm). (B) Example of fluorescence intensity of microtubules in
517 "B", connecting pMTOCs, mcMTOCs and the cortex, using the 'plot profiles' function in

518 ImageJ. The scale bar represents 10 µm. (C) Representative images (Z-projection of 16 sections
519 every 3 µm) of time-lapse confocal microscopy of a live oocyte expressing AURKA-GFP
520 (MTOCs) and H2B-mCherry (chromosomes) from a time course (see Supplemental Movie 7).
521 Fluorescence and bright-field images (lower panels) were captured every 20 min (time, h:min).
522 Arrowheads represent mcMTOCs. Scale bars represent 10 µm. (D) Schematic diagram shows
523 how the proportion of polar body extrusion side in relation to mcMTOC position was assessed.
524 (E) Quantification of the proportion of polar body extrusion side from "C" according to "D". The
525 data are expressed as mean ± SEM. Student t-test was used to analyze the data. Values with
526 asterisks vary significantly, ****$P < 0.0001$. The total number of analyzed oocytes (from three
527 independent replicates) is specified above the graph.
528
529 **Figure 4: mcMTOCs are required to regulate spindle positioning in meiotic**
530 **oocytes.** (A) Schematic diagram shows the experimental design following mcMTOC depletion.
531 (B-G) Oocytes expressing AURKA-GFP and eGFP-EB3 were *in vitro* maturated for 6 h
532 (metaphase I, Met I), transferred to CZB medium with or without MG-132, followed by
533 mcMTOC depletion using two-photon laser ablation. Small square area(s) surrounding
534 mcMTOCs were marked and then exposed to a laser with 927 nm wavelength. Control oocytes
535 were exposed to the same parameters except ablating random areas of the cytoplasm, just
536 adjacent and equal to the same size and number of mcMTOCs. (B**)** Z-sections of 3D time-lapse
537 imaging of a live oocyte during mcMTOC ablation (see Supplemental Movie 8). Black
538 arrowheads represent mcMTOCs before ablation (upper panels). White arrowheads represent
539 laser beam targets (middle panels). (C) Z-sections of 3D time-lapse imaging of live oocyte to
540 track microtubules (eGFP-EB3) following mcMTOC ablation. Black arrow represents mcMTOC

541 before ablation (-3 S). Black arrowheads track microtubules over time. The scale bar represents
542 20 μm. (D) control and mcMTOC-depleted oocytes were *in vitro* matured in MG-132-free
543 medium until Met II (16 h) and assessed for extrusion of the first polar body (PBE). The data are
544 expressed as mean ± SEM. chi-square contingency test was used to analyze the data. Values with
545 asterisks vary significantly, **P < 0.01. The total number of analyzed oocytes in each group
546 (from two independent replicates) is specified above each condition within each graph. (E) Z-
547 projection (16 sections every 3 μm) of 3D time-lapse microscopy of control (see Supplemental
548 Movie 9) and mcMTOC-depleted (see Supplemental Movie 10) Met I oocytes while cultured in
549 MG-132-containing medium for additional 9 h to track the spindle. Fluorescence images were
550 captured every 3 min (time, h:min). White arrowheads represent the tracking path of all time
551 periods. The scale bar represents 10 μm. (F) Quantification of total distance traveled by the
552 spindle. (G) Quantification of average spindle speed. The data are expressed as mean ± SEM.
553 Student t-test was used to analyze the data. Values with asterisks vary significantly, ****P <
554 0.0001. The total number of analyzed oocytes (from two independent replicates) is specified
555 above each graph.
556
557 **Figure 5: Autophagy regulates mcMTOC numbers in meiotic oocytes.** (A) Full-grown
558 prophase-I oocytes were divided into two groups and treated with DMSO or Rapamycin (added
559 at 0 h after collection) followed by *in vitro* maturation until metaphase I (Met I, 7h). Met I
560 oocytes were fixed and immunostained using Cep192 and α-tubulin antibodies to label MTOCs
561 (red) and microtubules (grey). DAPI was used to detect DNA (blue). (B) Quantification of
562 average mcMTOC number in "A". (C) Quantification of average pMTOC number in "A". (D)
563 Full-grown prophase-I oocytes were divided into two groups and treated with DMSO or 3-MA

564 (added at NEBD) followed by *in vitro* maturation until metaphase I (Met I, 7h). Met I oocytes
565 were fixed and immunostained using Cep192 and α-tubulin antibodies to label MTOCs (red) and
566 microtubules (grey). DAPI was used to detect DNA (blue). (E) Quantification of average
567 mcMTOC number in "D". (F) Quantification of average pMTOC number in "D". Arrowheads
568 represent mcMTOCs. The data are expressed as mean ± SEM. Student t-test was used to analyze
569 the data. Values with asterisks vary significantly, *P < 0.05, ****P < 0.0001. The total number
570 of analyzed oocytes (from two independent replicates) is specified above each graph.
571

572 **Figure 6: Autophagy regulates spindle positioning in meiotic oocytes.**

573 (A) Z-projection (16 sections every 3 μm) of time-lapse imaging of DMSO, Rapamycin (Rap)
574 and 3-MA-treated oocytes (see Supplemental Movie 11, 12, 13 and 14, respectively). Images
575 were captured every 30 min. White arrows represent the direction of chromosome displacement.
576 Scale bars represent 10 μm. Lower panels of each group show the tracking path (blue) over time.
577 (B) Quantification of the percentage of first polar body extrusion (PBE). (C) Quantification of
578 the average time spent by chromosomes from the start of migration till reaching the cortex. (D)
579 Quantification of the total distance traveled by chromosomes from the start of migration until
580 reaching the cortex. (E) Quantification of average chromosome speed during migration. (F)
581 Quantification of the percentage of oocytes exhibiting abnormal spindle positioning and
582 orientation prior to reaching the oocyte cortex. Arrows represent the direction of chromosome
583 displacement. The data are expressed as mean ± SEM. One-way ANOVA was used to analyze
584 the data. Values with asterisks vary significantly, *P < 0.05, ***P < 0.001, ****P < 0.0001. The
585 total number of analyzed oocytes (from three independent replicates) is specified above each
586 graph.

587 **Figure 7: Schematic model for spindle positioning in the meiotic oocyte.**

588

589 **Supplementary Figure 1: AURKA-GFP foci colocalize with pericentriolar material protein**

590 **(γ-tubulin) at mcMTOCs.** Full-grown prophase-I oocytes were injected with *Aurka-*

591 *Gfp* (green), incubated in milrinone-containing CZB medium for 3 h, followed by *in vitro*

592 maturation. Metaphase I oocytes were fixed and immunostained using γ-tubulin antibody to label

593 MTOCs (red). DAPI was used to detect DNA (blue). Shown are representative Z-projection of

594 confocal images. The scale bar represents 10 μm.

595

596 **Supplementary Figure 2: MTOCs in the cytoplasm and at the spindle poles of meiotic**

597 **oocytes collected from C57BL/6 mice.** Full-grown prophase-I oocytes collected from C57BL/6

598 mice were *in vitro* matured for 7 h. Metaphase I oocytes were fixed and immunostained using γ-

599 tubulin and α-tubulin antibodies to label MTOCs (red) and microtubules (grey). DAPI was used

600 to detect DNA (blue). Arrowheads represent mcMTOCs. Shown are representative Z-projection

601 of confocal images. The scale bar represents 10 μm.

602

603 **Supplementary Figure 3: mcMTOC movement does not follow the movement of the**

604 **cytoplasm.** Representative images (Z-projection of 16 sections every 3 μm) of time-lapse

605 confocal microscopy of live oocytes expressing AURKA-GFP (MTOCs) and H2B-mCherry

606 (chromosomes) from a time course. Fluorescence and bright-field images (lower panels) were

607 captured every 15 min (time, h:min). The white arrow represents cytoplasmic droplet. Lower

608 panels show the tracking of both cytoplasmic droplet (green) and mcMTOC (blue). The scale bar

609 represents 10 μm.

610 **Supplementary Figure 4: F-actin localization in mouse oocytes.** Full-grown prophase-I
611 oocytes collected from C57BL/6 mice were *in vitro* matured for 7 h. Metaphase I oocytes were
612 fixed and immunostained using γ-tubulin to label MTOCs (red). Hoechst stain was used to detect
613 DNA (blue) and phalloidin stain was used to detect F-actin (pseudo green). Shown are
614 representative Z-projection. The scale bar represents 10 μm.
615
616 **Supplementary Figure 5: Inhibition of MTs accelerates chromosome migration towards the**
617 **cortex in meiotic oocytes.** Full-grown prophase-I oocytes were divided into two groups and
618 treated with DMSO or nocodazole (added at 0 h after collection) followed by *in vitro* maturation
619 and time-lapse imaging. Images were captured every 15 min. (A) Quantification of the average
620 time spent by chromosomes until reaching the cortex. (B) Quantification of average chromosome
621 speed during migration. The data are expressed as mean ± SEM. Student-t test was used to
622 analyze the data. Values with asterisks vary significantly, ***$P < 0.001$, ****$P < 0.0001$. The
623 total number of analyzed oocytes (from two independent replicates) is specified above each
624 graph.
625
626 **Supplementary Figure 6: Two-photon laser ablation efficiently depletes mcMTOCs.**
627 Oocytes expressing AURKA-GFP and eGFP-EB3 were *in vitro* maturated for 6 h (metaphase I,
628 Met I), transferred to CZB medium with MG-132, followed by mcMTOC depletion using two-
629 photon laser ablation. Small square area(s) surrounding mcMTOCs were marked and then
630 exposed to a laser with 927 nm wavelength. Control oocytes were exposed to the same
631 parameters except ablating random areas of the cytoplasm, just adjacent and equal to the same
632 size and number of mcMTOCs. Control and mcMTOC-ablated oocytes were fixed and

633 immunostained using γ-tubulin antibody to label MTOCs. DAPI was used to detect DNA (blue).
634 Arrowheads represent mcMTOCs. Shown are representative Z-projection of confocal images.
635 The scale bar represents 10 μm.
636
637 **Supplementary Movie 1:** Time-lapse confocal microscopy of MTOCs in live oocyte. The
638 full-grown prophase-I oocyte was injected with cRNAs encoding *H2b-mCherry* (red) and *Aurka-*
639 *Gfp* (pseudo grey), followed by *in vitro* maturation. Fluorescence images (Z-projection of 16
640 sections every 3 μm) were captured every 20 min (time, h:min). Same oocyte as shown in Fig.
641 1A (upper panels). The scale bar represents 10 μm.
642
643 **Supplementary Movie 2:** 3D reconstruction of MTOCs from the oocyte in Supplementary
644 Movie 1. Same oocyte as shown in Fig. 1B (lower panels).
645
646 **Supplementary Movie 3:** 3D reconstruction of MTOCs from the oocyte in Supplementary
647 Movie 1 during metaphase I.
648
649 **Supplementary Movie 4:** Time-lapse confocal microscopy of MTOCs in live oocyte. The
650 full-grown prophase-I oocyte was injected with cRNAs encoding *H2b-mCherry* (red) and *Aurka-*
651 *Gfp* (pseudo grey), followed by *in vitro* maturation. Fluorescence images (Z-projection of 16
652 sections every 3 μm) were captured every 15 min (time, h:min). The scale bar represents 20 μm.
653 **Supplementary Movie 5:** Tracking of 3D reconstructed mcMTOCs from the oocyte in
654 Supplementary Movie 4 during nuclear envelope breakdown (NEBD) to early metaphase I (Met
655 I). Same oocyte as shown in Fig. 2A.

656

657 **Supplementary Movie 6:** Tracking of 3D reconstructed mcMTOCs from the oocyte in
658 Supplementary Movie 4 during late metaphase I to telophase I. Same oocyte as shown in Fig.
659 2C.

660

661 **Supplementary Movie 7:** Time-lapse confocal microscopy of MTOCs in live oocyte. The
662 full-grown prophase-I oocyte was injected with cRNAs encoding *H2b-mCherry* (red) and *Aurka-*
663 *Gfp* (pseudo grey), followed by *in vitro* maturation. Fluorescence and bright-field images (Z-
664 projection of 16 sections every 3 μm) were captured every 20 min (time, h:min). Same oocyte as
665 shown in Fig. 3C (lower panels). The scale bar represents 10 μm.

666

667 **Supplementary Movie 8:** 3D time-lapse imaging of live oocyte expressing AURKA-GFP
668 (pseudo grey) and eGFP-EB3 (pseudo grey) during mcMTOC ablation. The white squares
669 represent the actual laser beam targets. Same oocyte as shown in Fig. 4B.

670

671 **Supplementary Movie 9:** Tracking the spindle over time in control oocyte (non-mcMTOC-
672 ablated) expressing AURKA-GFP (pseudo grey) and eGFP-EB3 (pseudo grey), while cultured in
673 MG-132-containing medium for 9 h, using 3D time-lapse microscopy. Fluorescence images were
674 captured every 3 min (time, h:min). The scale bar represents 10 μm. Same oocyte as shown in
675 Fig. 4E.

676

677 **Supplementary Movie 10:** Tracking the spindle over time in mcMTOC-laser-ablated oocyte
678 expressing AURKA-GFP (pseudo grey) and eGFP-EB3 (pseudo grey), while cultured in MG-

679 132-containing medium for 9 h, using 3D time-lapse microscopy. Fluorescence images were
680 captured every 3 min (time, h:min). The scale bar represents 10 μm. Same oocyte as shown in
681 Fig. 4E.
682
683 **Supplementary Movie 11:** Tracking the chromosomes over time in DMSO-treated oocytes
684 during meiosis I. Bright-field images (Z-projection of 16 sections every 3 μm) were captured
685 every 30 min (time, h:min). Prophase -I stage represents 0 h. Same oocyte as shown in Fig. 6A
686 (Control). The scale bar represents 10 μm.
687
688 **Supplementary Movie 12:** Tracking the chromosomes over time in Rapamycin-treated
689 oocytes during meiosis I. Bright-field images (Z-projection of 16 sections every 3 μm) were
690 captured every 30 min (time, h:min). Prophase -I stage represents 0 h. Same oocyte as shown in
691 Fig. 6A (Rapamycin). The scale bar represents 10 μm.
692
693 **Supplementary Movie 13:** Tracking the chromosomes over time in 3-MA-treated oocytes
694 during meiosis I. Bright-field images (Z-projection of 16 sections every 3 μm) were captured
695 every 30 min (time, h:min). Prophase -I stage represents 0 h. Same oocyte as shown in Fig. 6A
696 (3-MA, upper panels). The scale bar represents 10 μm.
697
698 **Supplementary Movie 14:** Tracking the chromosomes over time in 3-MA-treated oocytes
699 during meiosis I (another representative showing defective asymmetrical division). Bright-field
700 images (Z-projection of 16 sections every 3 μm) were captured every 30 min (time, h:min).

701 Prophase -I stage represents 0 h. Same oocyte as shown in Fig. 6A (3-MA, lower panels). The

702 scale bar represents 10 μm.

703

704

705

706 **REFERENCES**

707 1 Von Stetina, J. R. & Orr-Weaver, T. L. Developmental control of oocyte maturation and
708 egg activation in metazoan models. Cold Spring Harb Perspect Biol 3, a005553,
709 doi:10.1101/cshperspect.a005553 (2011).
710 2 Hashimoto, N. & Kishimoto, T. Regulation of meiotic metaphase by a cytoplasmic
711 maturation-promoting factor during mouse oocyte maturation. Dev Biol 126, 242-252,
712 doi:10.1016/0012-1606(88)90135-2 (1988).
713 3 Bennabi, I., Terret, M. E. & Verlhac, M. H. Meiotic spindle assembly and chromosome
714 segregation in oocytes. J Cell Biol 215, 611-619, doi:10.1083/jcb.201607062 (2016).
715 4 Kitajima, T. S., Ohsugi, M. & Ellenberg, J. Complete kinetochore tracking reveals error-
716 prone homologous chromosome biorientation in mammalian oocytes. Cell 146, 568-581,
717 doi:10.1016/j.cell.2011.07.031 (2011).
718 5 McCarthy, E. K. & Goldstein, B. Asymmetric spindle positioning. Curr Opin Cell Biol
719 18, 79-85, doi:10.1016/j.ceb.2005.12.006 (2006).
720 6 Longo, F. J. & Chen, D. Y. Development of cortical polarity in mouse eggs: involvement
721 of the meiotic apparatus. Dev Biol 107, 382-394 (1985).
722 7 Menezo, Y. J. Paternal and maternal factors in preimplantation embryogenesis:
723 interaction with the biochemical environment. Reprod Biomed Online 12, 616-621,
724 doi:10.1016/s1472-6483(10)61188-1 (2006).
725 8 Ma, J., Zeng, F., Schultz, R. M. & Tseng, H. Basonuclin: a novel mammalian maternal-
726 effect gene. Development 133, 2053-2062, doi:10.1242/dev.02371 (2006).
727 9 Schuh, M. & Ellenberg, J. A new model for asymmetric spindle positioning in mouse
728 oocytes. Curr Biol 18, 1986-1992, doi:10.1016/j.cub.2008.11.022 (2008).
729 10 Azoury, J. et al. Spindle positioning in mouse oocytes relies on a dynamic meshwork of
730 actin filaments. Curr Biol 18, 1514-1519, doi:10.1016/j.cub.2008.08.044 (2008).
731 11 Li, H., Guo, F., Rubinstein, B. & Li, R. Actin-driven chromosomal motility leads to
732 symmetry breaking in mammalian meiotic oocytes. Nat Cell Biol 10, 1301-1308,
733 doi:10.1038/ncb1788 (2008).
734 12 McNally, F. J. Mechanisms of spindle positioning. J Cell Biol 200, 131-140,
735 doi:10.1083/jcb.201210007 (2013).
736 13 Szollosi, D., Calarco, P. & Donahue, R. P. Absence of centrioles in the first and second
737 meiotic spindles of mouse oocytes. J Cell Sci 11, 521-541 (1972).
738 14 Schuh, M. & Ellenberg, J. Self-organization of MTOCs replaces centrosome function
739 during acentrosomal spindle assembly in live mouse oocytes. Cell 130, 484-498,
740 doi:10.1016/j.cell.2007.06.025 (2007).
741 15 Xie, B. et al. Poly(ADP-ribose) mediates asymmetric division of mouse oocyte. Cell Res
742 28, 462-475, doi:10.1038/s41422-018-0009-7 (2018).
743 16 Schatten, H., Schatten, G., Mazia, D., Balczon, R. & Simerly, C. Behavior of
744 centrosomes during fertilization and cell division in mouse oocytes and in sea urchin
745 eggs. Proc Natl Acad Sci U S A 83, 105-109, doi:10.1073/pnas.83.1.105 (1986).
746 17 Verlhac, M. H., Lefebvre, C., Guillaud, P., Rassinier, P. & Maro, B. Asymmetric division
747 in mouse oocytes: with or without Mos. Curr Biol 10, 1303-1306 (2000).
748 18 Clift, D. & Schuh, M. A three-step MTOC fragmentation mechanism facilitates bipolar
749 spindle assembly in mouse oocytes. Nat Commun 6, 7217, doi:10.1038/ncomms8217
750 (2015).

751 19 Luksza, M., Queguigner, I., Verlhac, M. H. & Brunet, S. Rebuilding MTOCs upon
752 centriole loss during mouse oogenesis. Dev Biol 382, 48-56,
753 doi:10.1016/j.ydbio.2013.07.029 (2013).
754 20 Balboula, A. Z. et al. Haspin kinase regulates microtubule-organizing center clustering
755 and stability through Aurora kinase C in mouse oocytes. J Cell Sci 129, 3648-3660,
756 doi:10.1242/jcs.189340 (2016).
757 21 Breuer, M. et al. HURP permits MTOC sorting for robust meiotic spindle bipolarity,
758 similar to extra centrosome clustering in cancer cells. J Cell Biol 191, 1251-1260,
759 doi:10.1083/jcb.201005065 (2010).
760 22 Messinger, S. M. & Albertini, D. F. Centrosome and microtubule dynamics during
761 meiotic progression in the mouse oocyte. J Cell Sci 100 (Pt 2), 289-298 (1991).
762 23 Houliston, E., Pickering, S. J. & Maro, B. Redistribution of microtubules and
763 pericentriolar material during the development of polarity in mouse blastomeres. J Cell
764 Biol 104, 1299-1308, doi:10.1083/jcb.104.5.1299 (1987).
765 24 Meng, X. Q. et al. Localization of gamma-tubulin in mouse eggs during meiotic
766 maturation, fertilization, and early embryonic development. J Reprod Dev 50, 97-105,
767 doi:10.1262/jrd.50.97 (2004).
768 25 Maro, B., Houliston, E. & Paintrand, M. Purification of meiotic spindles and cytoplasmic
769 asters from mouse oocytes. Dev Biol 129, 275-282, doi:10.1016/0012-1606(88)90374-0
770 (1988).
771 26 Saskova, A. et al. Aurora kinase A controls meiosis I progression in mouse oocytes. Cell
772 Cycle 7, 2368-2376, doi:10.4161/cc.6361 (2008).
773 27 Solc, P. et al. Aurora kinase A drives MTOC biogenesis but does not trigger resumption
774 of meiosis in mouse oocytes matured in vivo. Biol Reprod 87, 85,
775 doi:10.1095/biolreprod.112.101014 (2012).
776 28 Bury, L. et al. Plk4 and Aurora A cooperate in the initiation of acentriolar spindle
777 assembly in mammalian oocytes. J Cell Biol 216, 3571-3590, doi:10.1083/jcb.201606077
778 (2017).
779 29 Gueth-Hallonet, C. et al. gamma-Tubulin is present in acentriolar MTOCs during early
780 mouse development. J Cell Sci 105 (Pt 1), 157-166 (1993).
781 30 So, C. et al. A liquid-like spindle domain promotes acentrosomal spindle assembly in
782 mammalian oocytes. Science 364, doi:10.1126/science.aat9557 (2019).
783 31 Ma, W. & Viveiros, M. M. Depletion of pericentrin in mouse oocytes disrupts
784 microtubule organizing center function and meiotic spindle organization. Mol Reprod
785 Dev 81, 1019-1029, doi:10.1002/mrd.22422 (2014).
786 32 Mogessie, B. & Schuh, M. Actin protects mammalian eggs against chromosome
787 segregation errors. Science 357, doi:10.1126/science.aal1647 (2017).
788 33 Brunet, S. & Maro, B. Germinal vesicle position and meiotic maturation in mouse oocyte.
789 Reproduction 133, 1069-1072, doi:10.1530/REP-07-0036 (2007).
790 34 Almonacid, M. et al. Active diffusion positions the nucleus in mouse oocytes. Nat Cell
791 Biol 17, 470-479, doi:10.1038/ncb3131 (2015).
792 35 Colin, A. et al. Active diffusion in oocytes nonspecifically centers large objects during
793 prophase I and meiosis I. J Cell Biol 219, doi:10.1083/jcb.201908195 (2020).
794 36 Almonacid, M. et al. Active Fluctuations of the Nuclear Envelope Shape the
795 Transcriptional Dynamics in Oocytes. Dev Cell 51, 145-157 e110,
796 doi:10.1016/j.devcel.2019.09.010 (2019).

797 37 Denk, W., Strickler, J. H. & Webb, W. W. Two-photon laser scanning fluorescence
798 microscopy. Science 248, 73-76, doi:10.1126/science.2321027 (1990).
799 38 Duncan, F. E., Chiang, T., Schultz, R. M. & Lampson, M. A. Evidence that a defective
800 spindle assembly checkpoint is not the primary cause of maternal age-associated
801 aneuploidy in mouse eggs. Biol Reprod 81, 768-776, doi:10.1095/biolreprod.109.077909
802 (2009).
803 39 Balboula, A. Z. & Schindler, K. Selective disruption of aurora C kinase reveals distinct
804 functions from aurora B kinase during meiosis in mouse oocytes. PLoS Genet 10,
805 e1004194, doi:10.1371/journal.pgen.1004194 (2014).
806 40 Watanabe, Y. et al. Autophagy controls centrosome number by degrading Cep63. Nat
807 Commun 7, 13508, doi:10.1038/ncomms13508 (2016).
808 41 Honda, S. & Shimizu, S. Autophagy controls centrosome number. Oncotarget 8, 14277-
809 14278, doi:10.18632/oncotarget.15362 (2017).
810 42 George, M. A., Pickering, S. J., Braude, P. R. & Johnson, M. H. The distribution of
811 alpha- and gamma-tubulin in fresh and aged human and mouse oocytes exposed to
812 cryoprotectant. Mol Hum Reprod 2, 445-456, doi:10.1093/molehr/2.6.445 (1996).
813 43 Roeles, J. & Tsiavaliaris, G. Actin-microtubule interplay coordinates spindle assembly in
814 human oocytes. Nat Commun 10, 4651, doi:10.1038/s41467-019-12674-9 (2019).
815 44 Schultz, R. M., Montgomery, R. R. & Belanoff, J. R. Regulation of mouse oocyte meiotic
816 maturation: implication of a decrease in oocyte cAMP and protein dephosphorylation in
817 commitment to resume meiosis. Dev Biol 97, 264-273, doi:10.1016/0012-
818 1606(83)90085-4 (1983).
819 45 Stein, P. & Schindler, K. Mouse oocyte microinjection, maturation and ploidy
820 assessment. J Vis Exp, doi:10.3791/2851 (2011).
821 46 Tsafriri, A., Chun, S. Y., Zhang, R., Hsueh, A. J. & Conti, M. Oocyte maturation
822 involves compartmentalization and opposing changes of cAMP levels in follicular
823 somatic and germ cells: studies using selective phosphodiesterase inhibitors. Dev Biol
824 178, 393-402, doi:10.1006/dbio.1996.0226 (1996).
825 47 Chatot, C. L., Ziomek, C. A., Bavister, B. D., Lewis, J. L. & Torres, I. An improved
826 culture medium supports development of random-bred 1-cell mouse embryos in vitro. J
827 Reprod Fertil 86, 679-688, doi:10.1530/jrf.0.0860679 (1989).
828 48 Shuda, K., Schindler, K., Ma, J., Schultz, R. M. & Donovan, P. J. Aurora kinase B
829 modulates chromosome alignment in mouse oocytes. Mol Reprod Dev 76, 1094-1105,
830 doi:10.1002/mrd.21075 (2009).
831 49 Bennabi, I. et al. Artificially decreasing cortical tension generates aneuploidy in mouse
832 oocytes. Nat Commun 11, 1649, doi:10.1038/s41467-020-15470-y (2020).

833

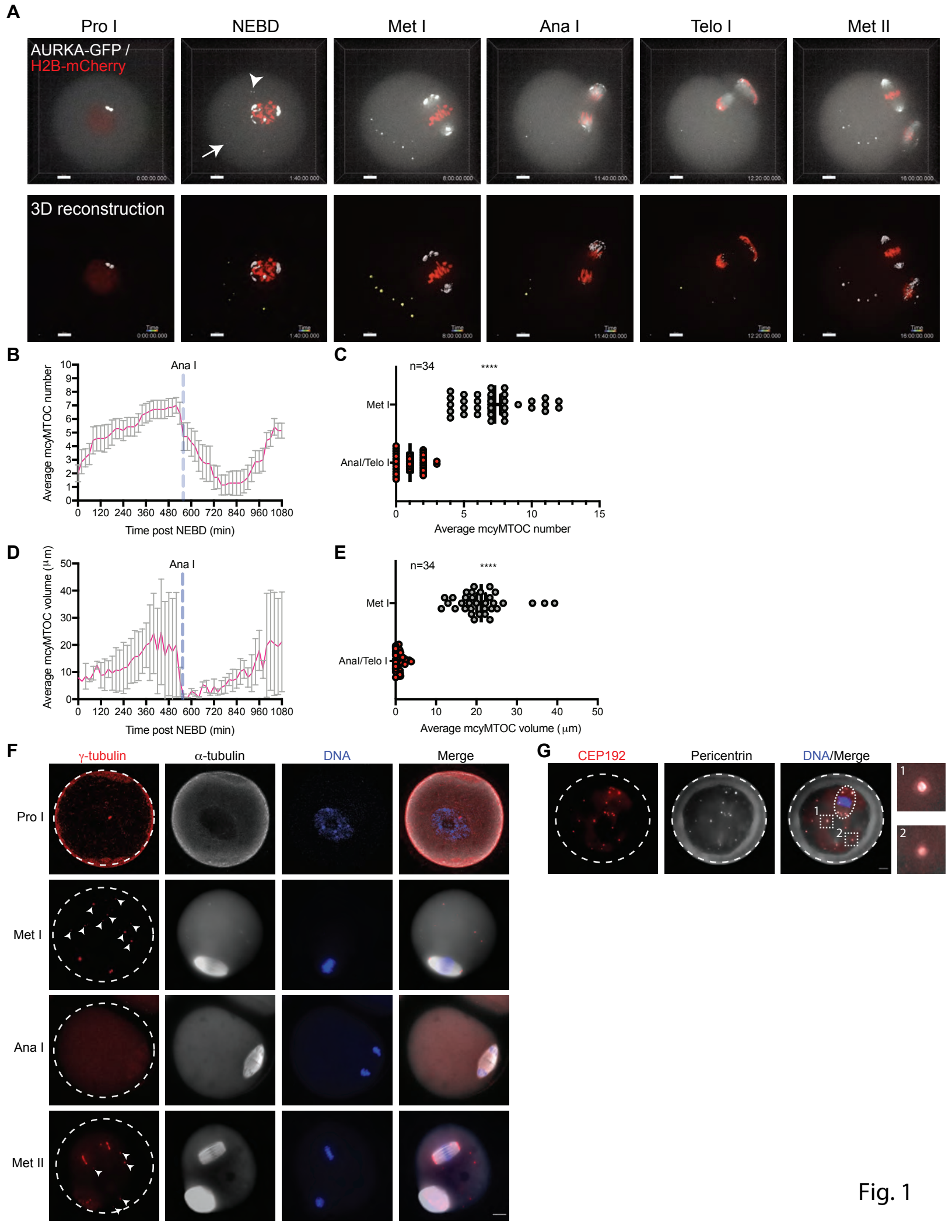
A
Pro I
NEBD
Met I
Ana I
Telo I
Met II
AURKA-GFP /
H2B-mCherry
3D reconstruction
B
Ana I
Average mcyMTOC number
Time post NEBD (min)
C
n=34
****
Met I
Anal/Telo I
Average mcyMTOC number
D
Ana I
Average mcyMTOC volume (μm)
Time post NEBD (min)
E
n=34
****
Met I
Anal/Telo I
Average mcyMTOC volume (μm)
F
γ-tubulin
α-tubulin
DNA
Merge
Pro I
Met I
Ana I
Met II
G
CEP192
Pericentrin
DNA/Merge
1
2

Fig. 1

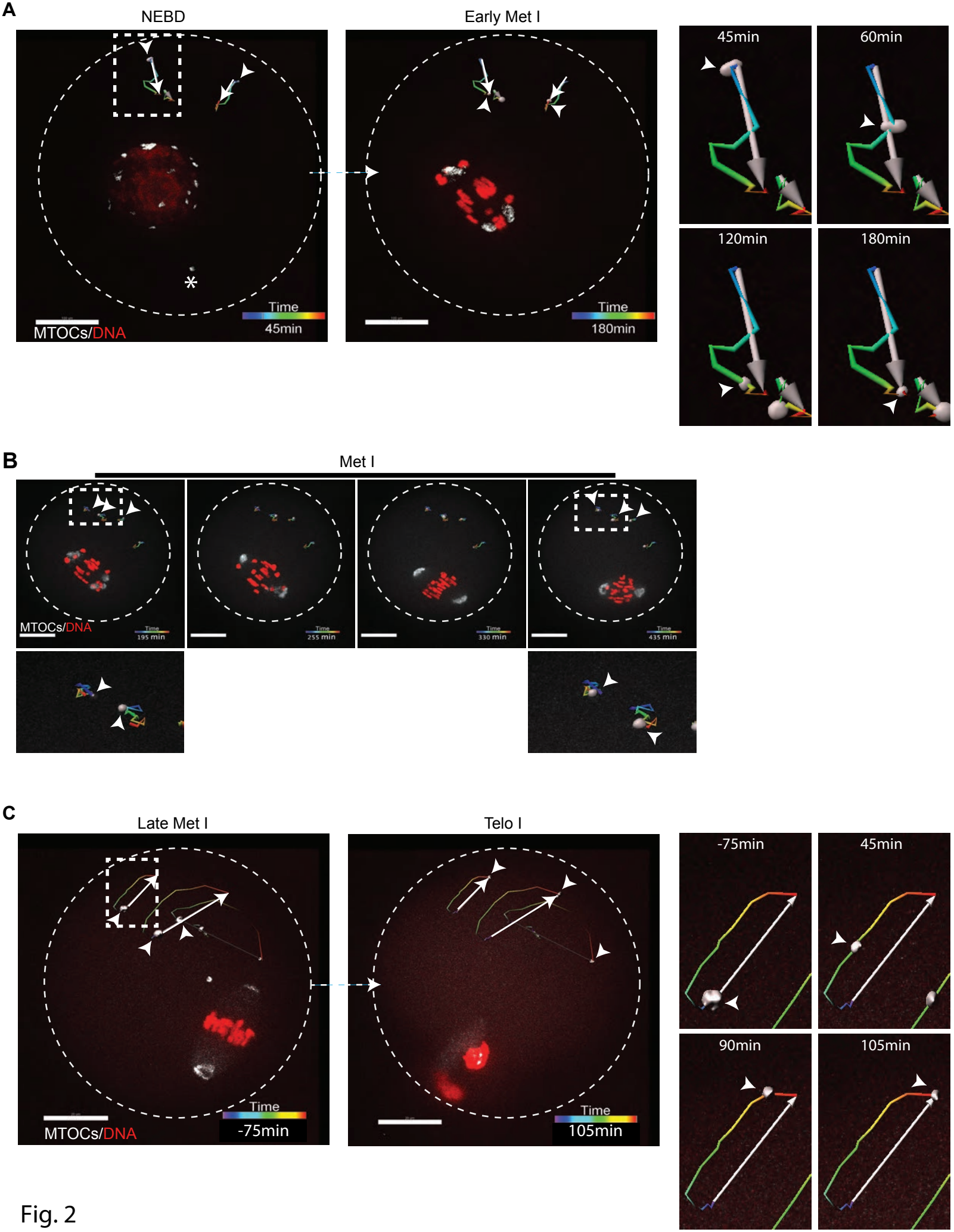
A
NEBD
Early Met I
45min
60min
120min
180min
Time
45min
MTOCs/DNA
Time
180min
B
Met I
MTOCs/DNA
Time
195 min
Time
255 min
Time
330 min
Time
435 min
C
Late Met I
Telo I
-75min
45min
90min
105min
Time
-75min
MTOCs/DNA
Time
105min

Fig. 2

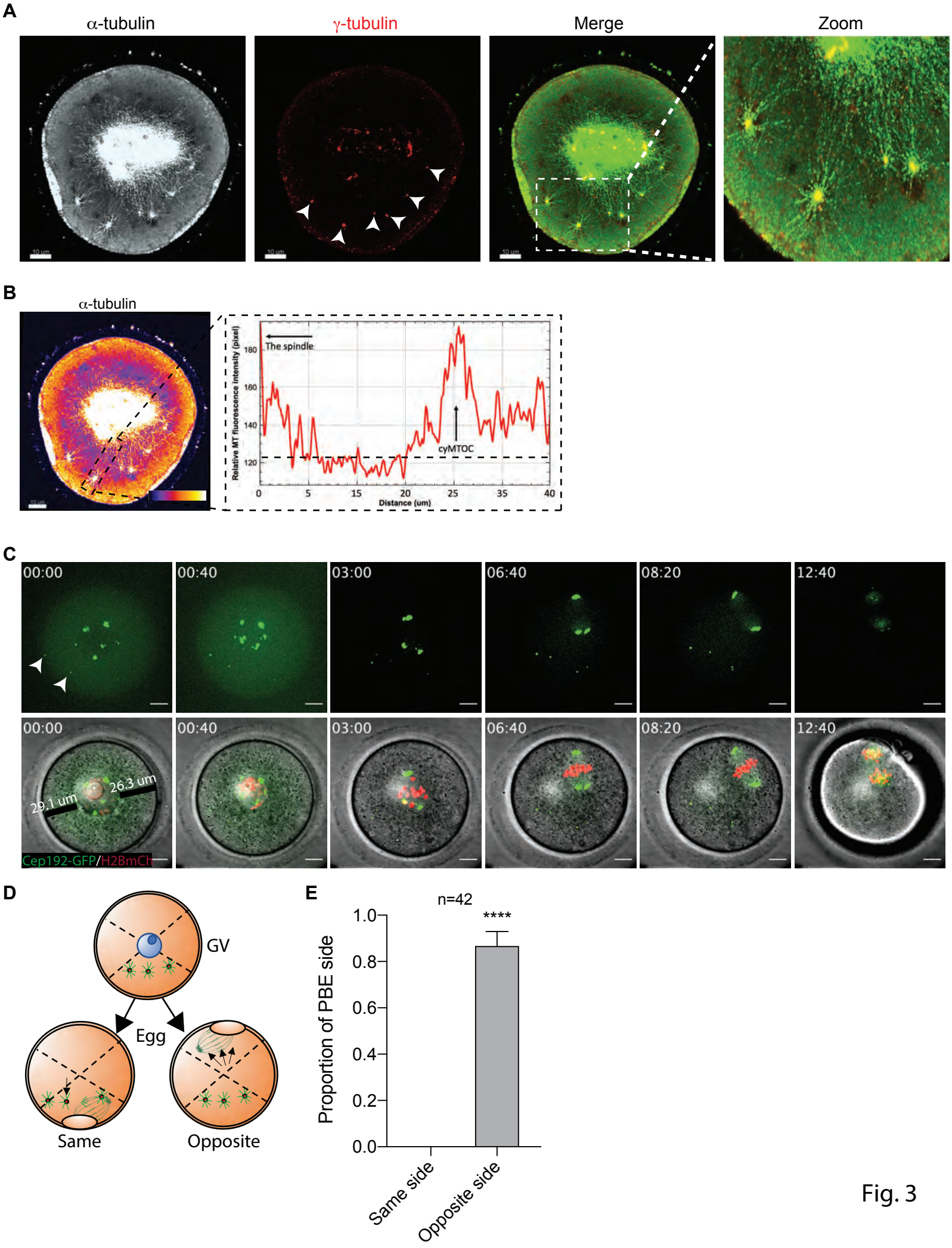
A
α-tubulin
γ-tubulin
Merge
Zoom
B
α-tubulin
The spindle
cyMTOC
Relative MT fluorescence intensity (pixel)
Distance (um)
C
00:00
00:40
03:00
06:40
08:20
12:40
29.1 um
26.3 um
Cep192-GFP/H2BmCh
D
GV
Egg
Same
Opposite
E
n=42
****
Proportion of PBE side
Same side
Opposite side

Fig. 3

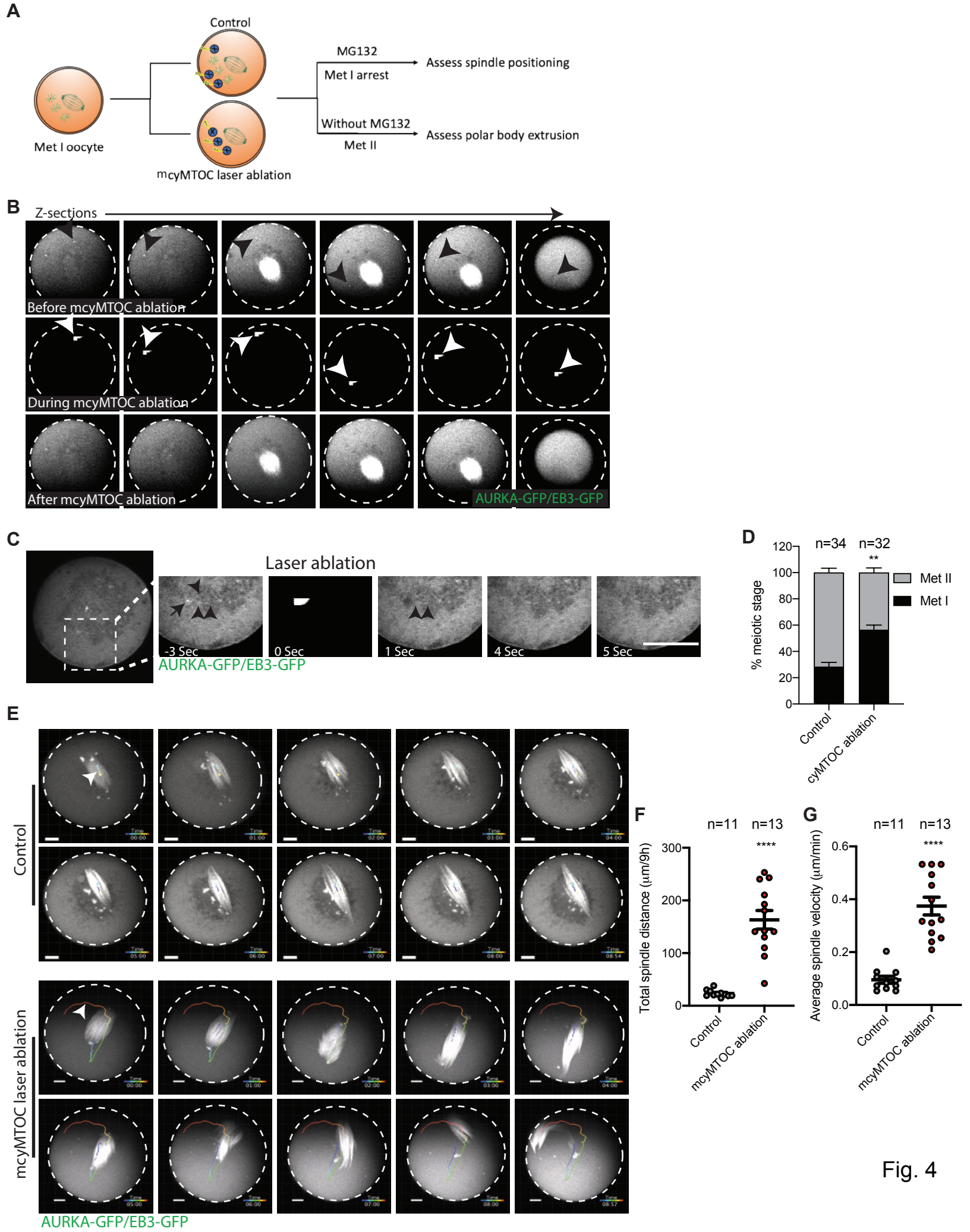
A
Control
MG132
Met I arrest
Assess spindle positioning
Met I oocyte
Without MG132
Met II
Assess polar body extrusion
mcyMTOC laser ablation
B
Z-sections
Before mcyMTOC ablation
During mcyMTOC ablation
After mcyMTOC ablation
AURKA-GFP/EB3-GFP
C
Laser ablation
-3 Sec
0 Sec
1 Sec
4 Sec
5 Sec
AURKA-GFP/EB3-GFP
D
n=34
n=32
**
Met II
Met I
% meiotic stage
Control
cyMTOC ablation
E
Control
mcyMTOC laser ablation
AURKA-GFP/EB3-GFP
F
n=11
n=13
****
Total spindle distance (µm/9h)
Control
mcyMTOC ablation
G
n=11
n=13
****
Average spindle velocity (µm/min)
Control
mcyMTOC ablation

Fig. 4

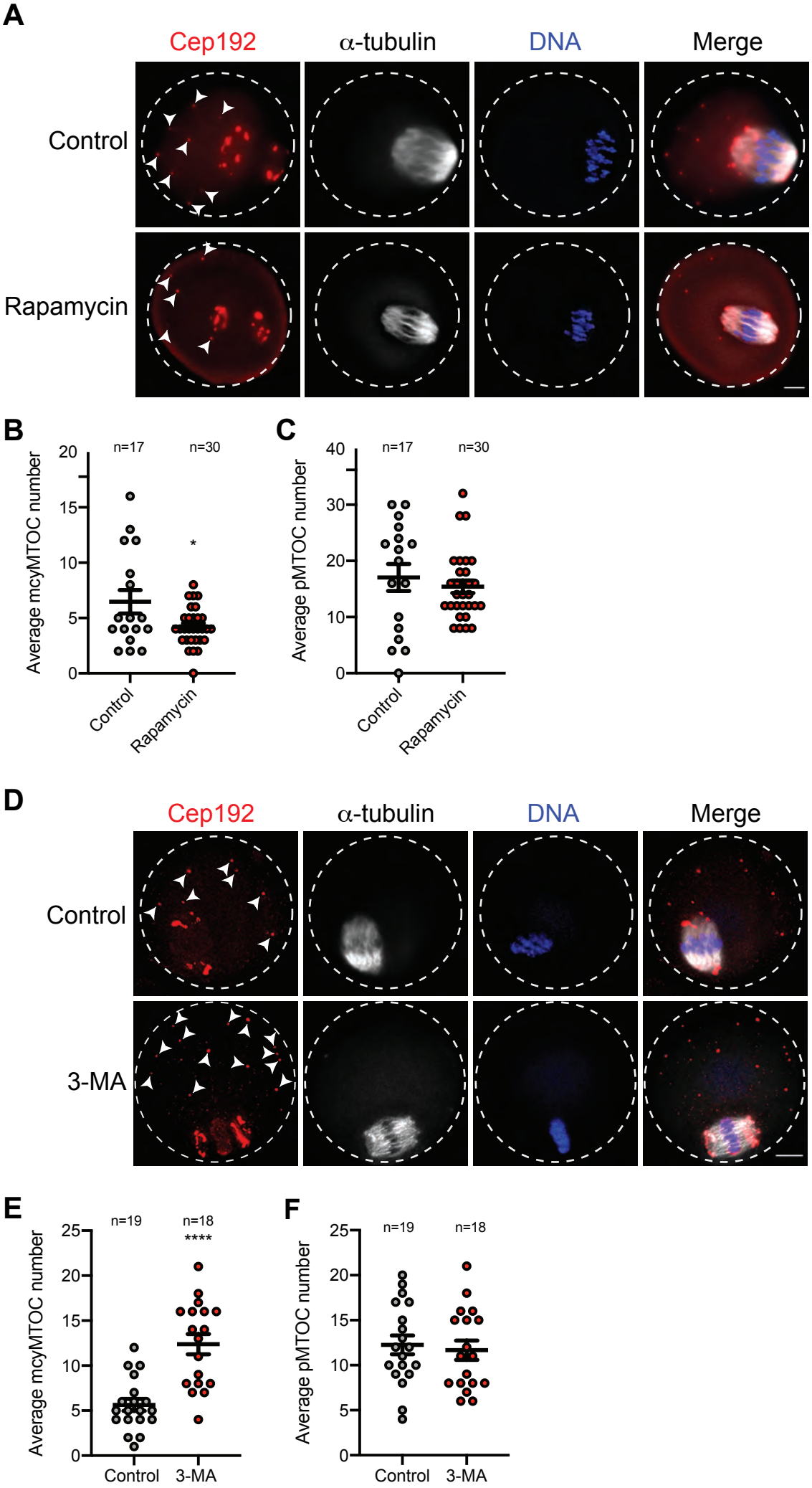
A
Cep192
α-tubulin
DNA
Merge
Control
Rapamycin
B
Average mcyMTOC number
n=17
n=30
*
Control
Rapamycin
C
Average pMTOC number
n=17
n=30
Control
Rapamycin
D
Cep192
α-tubulin
DNA
Merge
Control
3-MA
E
Average mcyMTOC number
n=19
n=18
****
Control
3-MA
F
Average pMTOC number
n=19
n=18
Control
3-MA

Fig. 5

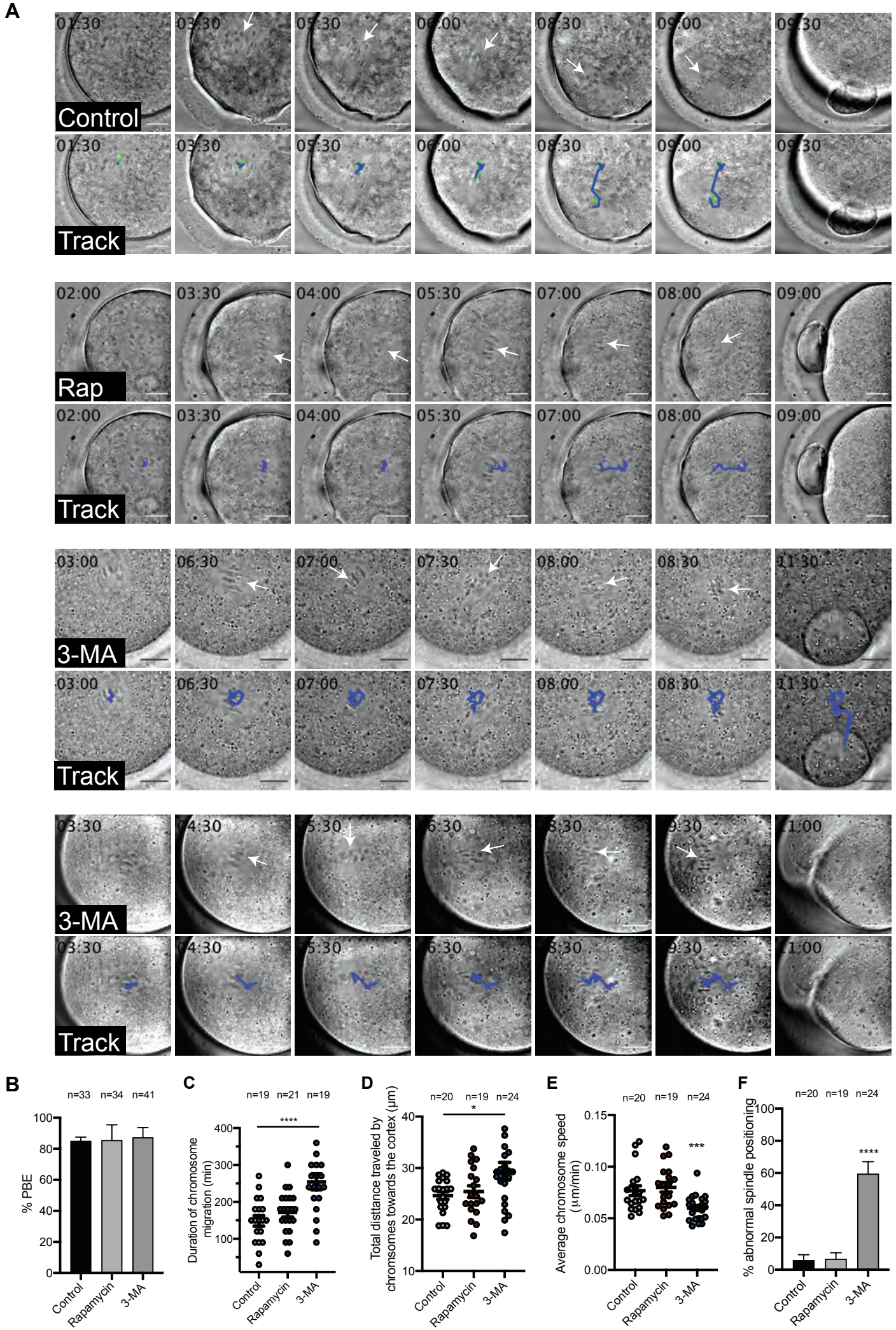
A
Control
Track
Rap
Track
3-MA
Track
3-MA
Track
B
n=33 n=34 n=41
% PBE
Control
Rapamycin
3-MA
C
n=19 n=21 n=19
****
Duration of chromosome migration (min)
Control
Rapamycin
3-MA
D
n=20 n=19 n=24
*
Total disttance traveled by chromsomes towards the cortex (μm)
Control
Rapamycin
3-MA
E
n=20 n=19 n=24
***
Average chromosome speed (μm/min)
Control
Rapamycin
3-MA
F
n=20 n=19 n=24
****
% abnormal spindle positioning
Control
Rapamycin
3-MA

Fig. 6

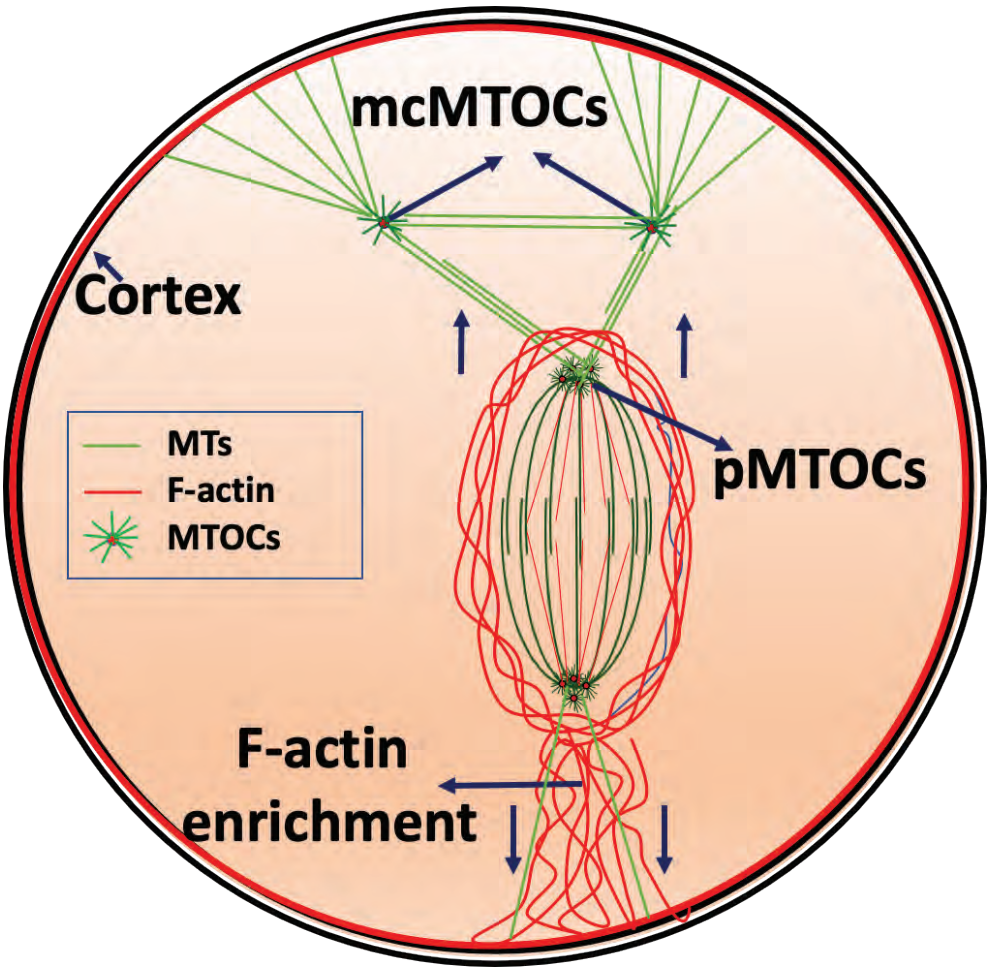

Fig. 7